2018-01-11

Block and boulder accumulations on the southern coast of Crete (Greece): evidence for the 365 CE tsunami in the Eastern Mediterranean

Boulton, Sarah

10.1144/SP456.4
The Geological Society

Block and boulder accumulations on the southern coast of Crete (Greece): evidence for the 365 CE tsunami in the Eastern Mediterranean.

Sarah J. Boulton[1*], Michael R.Z. Whitworth[1, 2],

[1]School of Geography, Earth and Environmental Sciences, Plymouth University, Plymouth, Devon, PL4 8AA, U.K.

[2] *AECOM*, Mayflower House, Armada Way, Plymouth, Devon, PL1 1LD.

*Correspondence (sarah.boulton@plymouth.ac.uk)

The Eastern Mediterranean is one of the most seismically active regions in Europe. Crete, located in the centre of the Eastern Mediterranean, should experience tsunamis resulting from large magnitude earthquakes or volcanic eruptions. At three locations boulders were observed that may relate to tsunami or storm events. At Lakki, the size of the boulders slightly favours a tsunami origin for deposition. By contrast, at Kommos boulder size and geomorphology is consistent with storm parameters in the Mediterranean. The most compelling evidence for tsunami transport is found at Diplomo Petris, where a lithologically varied grouping of large boulders (≤ 690 t) is exposed at sea level. The calculated storm wave heights (15 m) required to transport the observed boulders significantly exceeds winter averages; therefore, these accumulations are interpreted as tsunami deposits. Radiocarbon dating of encrusting biological material was undertaken to constrain periods of boulder motion. Encrustations from Diplomo Petris and Lakki pre-date the 365 CE earthquake suggesting that this event transported the largest boulders; the first time boulder deposits have been identified on Crete from this tsunami. Therefore, these data are important for developing local and regional hazard assessments but also to inform numerical models of tsunami propagation in the Mediterranean.

Keywords: tsunami; boulder; Eastern Mediterranean; Hellenic Arc; Photogrammetry; Extreme value analysis

In recent years there has been increased interest in coastal boulder accumulations worldwide and the recognition that these deposits are not only the result of high frequency storm processes but also of low frequency tsunami events (i.e., Dawson, 1994; Dawson & Shi, 2000; Bryant & Nott, 2001; Nott, 2003a; b; Kennedy *et al*., 2007). Interest in boulder deposits was sparked in the aftermath of the 2004 Boxing Day Indian Ocean tsunami as a result of the extensive boulder transport witnessed (e.g., Etienne *et al*., 2011). Although determining the transport history and origin of coastal boulders remains challenging, a range of criteria and characteristics that can be used to separate storm from tsunami deposits are beginning to emerge from the study of recent events (e.g., Scheffers, 2008).

In Thailand, boulders derived from coastal defences and natural settings, such as reefs and beachrock, were observed to have been transported up to 900 m inland in fields of scattered boulders with local imbrication or lines of deposition, so called 'boulder trains' (Goto *et al*., 2007; Paris *et al*., 2009, 2010). Paris *et al*. (2009) reported the presence of landward imbricated tabular boulders in Indonesia, while Paris *et al*. (2010) also documented that there was no relationship between boulder size and transport distance.

Extensive boulder deposits were also reported from the 2009 South Pacific tsunami affecting American Samoa and other South Pacific islands (Etienne *et al*., 2011). Richmond *et al*. (2011a) described a well-developed boulder field with no trend in boulder size distribution and with boulder long axes perpendicular to the flow direction. While, Goto *et al*. (2012) documented tuffaceous and concrete boulders that were observed to have been reworked from sea defences and rockfalls after the 2011 Tohoku-oki tsunami, Japan, observing that platy concrete boulders exhibited a landward fining in clast size as well as landward imbrication. By contrast, the blocky tuffaceous boulders showed either a landward coarsening in clast size or no trend in clast size distribution. These differences were interpreted to be the result of the concrete slabs being transported and deposited by the incoming flow and the light tuffaceous blocks during the return flow (Goto *et al*., 2012). This suggests that the lack of size trends observed elsewhere maybe due to a combination of boulder transport and deposition during the incoming and outgoing flow (Bahlburg & Spiske, 2012). Nandasena *et al*., (2013) also measured boulders following the 2011 Japanese earthquake in northern Japan, demonstrating that the long axes of the boulders was broadly perpendicular to transport direction. Similar relationships have been observed after the 2004 Indian Ocean tsunami (Goto *et al*., 2007; Etienne *et al*., 2011), the 2009 South Pacific Tsunami (Richmond *et al*., 2011a), on Hawaii (Richmond et al., 2011b) as well as in ancient deposits (i.e., Ramalho *et al*., 2015).

These characteristics are somewhat different to the boulder beaches, ridges and ramparts that appear to be characteristic of storm-derived boulder accumulations (e.g., Oak, 1984; Kortekaas & Dawson, 2007; Morton *et al*., 2007; 2008; Etienne & Paris, 2010; Paris *et al*., 2011). In comparison, tsunamis form distributed debris fields not the stratified, shore parallel ridges associated with storm waves (Morton *et al*., 2008). Furthermore, Etienne and Paris (2010) showed that storm boulder beaches generally show a landward decrease in boulder size, imbrication may be present, and the shape and size of clasts reflects the lithology of the underlying bedrock.

Therefore, we can summarise that tsunami boulders could be recognised by their large size that cannot be explained easily by known storm parameters for the study areas (e.g., Goto *et al*., 2010), a lack of grain size trends along the flow direction, yet orientation of the boulder long axis perpendicular to flow direction. The imbrication of large boulders may also be significant and has been used as a tsunami indicator (Kennedy *et al*., 2007; Maouche *et al*., 2009) but equally has also been recognised in storm boulder deposits (Morton *et al*., 2008; Etienne & Paris, 2010). Furthermore, evidence of a littoral or foreshore origin for boulders displaced far inland is also an important tsunami signature (Scheffers & Scheffers, 2007) but not unique as storm transported boulders can also originate in the near shore; features that can be used as diagnostic indicators of a marine origin include calcareous algal encrustations, bivalve borings, bioerosive notches and tilted rock pools (Scheffers, 2008). Finally, these geometrical observations and interpretations can be tested by the use of hydrodynamic models, such as those of Nott (1997, 2003a, b), Nandasena *et al*., (2011), and Benner *et al*. (2010), to determine the wave heights and velocities needed to transport observed boulders.

Numerous studies have attempted to recognise palaeo-tsunami deposits using these characteristics (e.g., Nott, 1997; Kelletat *et al*., 2004; Goff *et al*., 2006; Kennedy *et al*., 2007; Shah-hosseini *et al*., 2012; Hoffman *et al*., 2013; Ramalho *et al*., 2015) but are hampered in study areas where significant storm wave heights can be generated (i.e., May et al., 2015), complicating the distinction between tsunami and storm deposits through overlap in calculated wave heights needed for transport and reworking of boulder deposits. However, the Mediterranean basin offers a good opportunity for the study of palaeo-tsunamis due to a micro-tidal regime, limited fetch reducing maximum possible storm wave heights and many active faults and other tsunamigenic sources. As a result tsunami boulder

deposits have been described from across the Mediterranean region [Algeria (Maouche *et al*., 2009), France (Vella *et al*., 2011), Sicily (Scicchitano et al., 2007; Barbano *et al*., 2010) and the Adriatic (Mastronuzzi & Sanso, 2004), Malta (Mottershead *et al*., 2014; 2015); Cyprus (Kelletat & Schellmann, 2002) and Greece (Scheffers & Scheffers, 2007; Scheffers *et al*., 2008; Vacchi *et al*., 2012)]. In addition, fine-grained to cobble deposits attributed to tsunamis are also common in the Mediterranean and have been described mainly from Italy, Greece and Turkey (i.e., Dominey-Howes, 1998; Vött *et al*., 2007, 2008, 2009, 2011; Bruins *et al*., 2008; May *et al*., 2012; Smedile *et al*., 2011, 2012).

Here we document locations from southern Crete where unusual boulder accumulations were observed. This study focusses on boulder accumulations for two reasons; firstly, the coarsest grainsize fraction is required to determine maximum flow characteristics, such as velocity and wave height, that can be used to test numerical models. The fine-grained fractions washed further inland cannot give information on these parameters. Secondly, the southern coast of Crete is dominated by steep mountainous topography with deeply incised drainage lines unsuitable for the preservation of fine-grained material. Qualitative and quantitative evidence is described and combined with recent wave data and radiocarbon dating to interpret these accumulations in terms of storm or tsunami wave processes. These data provide important data for future validation of tsunami models for the Mediterranean region.

Geological Setting

The island of Crete, located at the centre of the Hellenic Arc, is the topographic expression of the accretionary wedge above the subducting African plate below the Eurasian plate. The Hellenic boundary accommodates ~ 40 $mmyr^{-1}$ of relative motion between the African and Eurasian plates (Reilinger *et al*., 2006; Nocquet, 2012). This fast plate convergence rate corresponds to high levels of historical and recent seismicity, with ≤ 20 % of the relative plate motion accommodated as earthquakes (Vernant *et al*., 2014) with remainder of the plate motion occurring through aseismic slip (Reilinger *et al*., 2010).

Therefore, Crete should have been affected by the numerous recorded tsunamigenic earthquakes that have occurred in the region since antiquity (e.g., Kelletat & Schellmann, 2002; Ambraseys & Synokis, 2010; England *et al*., 2015) and an unknown number in Pre-history (Fig. 1). In addition, tsunamis caused by volcanic eruptions also have the potential to affect this coast (Dominey-Howes *et al*., 2000). However, many of these events were small in nature, or of dubious provenance (Ambraseys & Synolakis, 2010). Yet there is clear evidence for at least five large tsunamigenic earthquakes along the Hellenic plate boundary zone where earthquake magnitudes exceeded M = 7 (Fig. 1). These devastating tsunamis took place on 21 July 365 CE, Crete; 8 August 1303 CE, Crete; 3 May 1481 CE, Rhodes; 28 February 1629 CE, Kythera, and 22 January, 1899 CE, Kyparissia (England *et al*., 2015).

However, up to now only traces of the tsunami generated by the eruption of Santorini in ~ 1650 BCE have been observed in the far east of the island (Bruins *et al*., 2008) and a series of fine-grained tsunami deposits have been observed in and nearby the ancient harbour of Phalasarna in the far west of Crete, dating to tsunamis that occurred in 66 CE and 365 CE (Pirazzoli *et al*., 1992; Stiros & Papageorgiou, 2001; Scheffers & Scheffers, 2007). Boulder clusters have also been described by Scheffers and Scheffers (2007) in western Crete but limited dating suggests only that these deposits

are probably younger than 365 CE. Furthermore, investigations by Dominey-Howes (2004) failed to document any tsunami traces along the north coast of Crete. This lack of geological evidence for extreme events seems rather incongruous given the evidence for large tsunamis in the region.

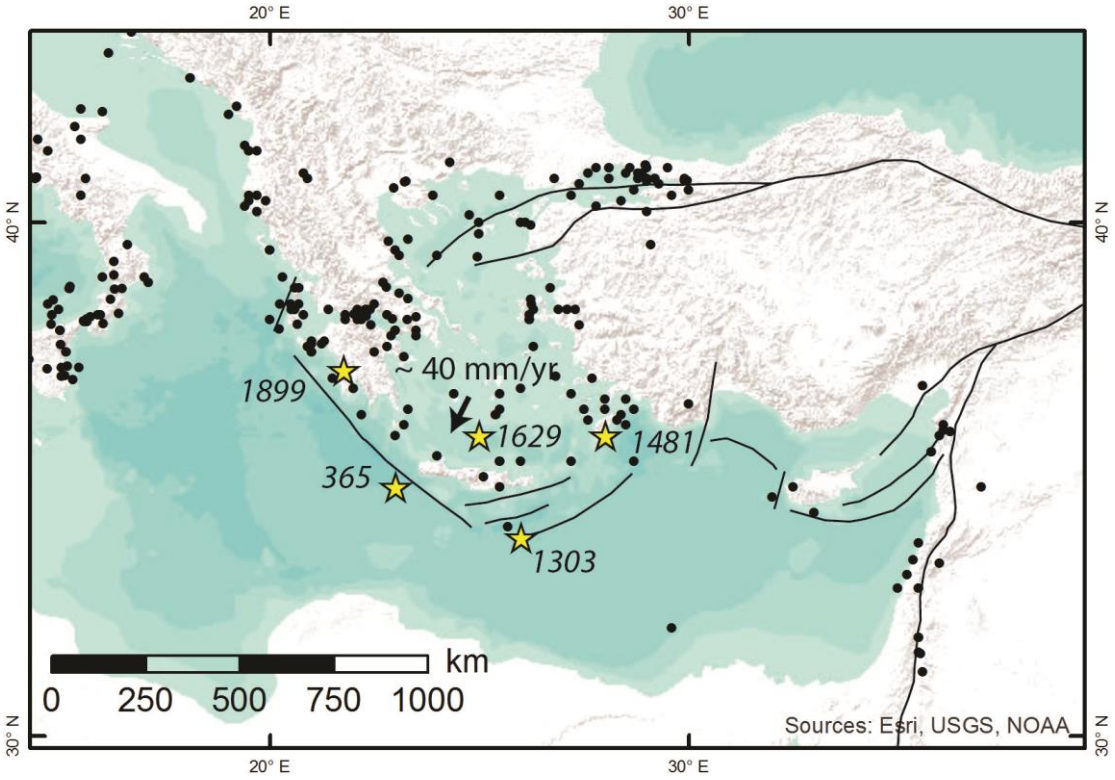

Figure 1. Distribution of tsunami source events from 2000 BCE to 2004 CE in the eastern Mediterranean (NGDC/WDS, 2015), stars indicate the sources of the five largest tsunamigenic events according to England et al., (2015).

One of the largest earthquakes ever documented for the Mediterranean was the ~M_w=8, 365 CE earthquake and tsunami (Pirazzoli, 1986; Pirazzoli *et al*., 1996; Shaw *et al*., 2008), which caused the coast of Crete to be uplifted by as much as 9 m absl, as evidenced by a raised marine notch observed across western Crete (Pirazzoli *et al*., 1996). The event also generated a tsunami that caused devastation throughout the Eastern Mediterranean, especially along the north coast of Africa (e.g., Guidoboni *et al*., 1994; Ambraseys & Synolakis, 2010). The location of the fault causing this rupture is still under debate but there are a number of numerical models using a shallow thrust ramp (~ 30° dip) within the upper Aegean plate as the causative fault (i.e., Shaw *et al*., 2008; Papadimitriou & Karakostas, 2008; England *et al*., 2015), while others suggest that the plate interface ruptured (i.e., Ganas & Parsons, 2009; Stiros, 2010). Similar debates exist regarding the location and morphology of the causative faults for the other major plate boundary earthquakes (England *et al*., 2015). Therefore, new field data are required in order that models of tsunami propagation and fault structure can be tested and refined.

Methods

Sedimentology

In this study >75 km of coastline along the southern edge of Crete (Fig. 2) was investigated for evidence of tsunami deposits. This area was targeted due to the small amount of vertical uplift (~0 – 2 m) felt in this region as a result of the 365 CE earthquake (Fig. 2). As this area did not experience significant uplift it is more likely to record tsunami deposits from this event as well as possible tsunamis that predate and postdate this event. Furthermore, due to the generally steep and mountainous topography of the southern coast there is less tourist development than elsewhere on the island. However, this rugged geomorphology also means there are few areas where fine-grained tsunami sediments could accumulate and so the focus of this study was on potential tsunami boulder deposits and care had to be taken to rule out material from rock falls.

In particular, sediments from the littoral or foreshore that now occupy an onshore position were examined and measured (maximum length of a, b, c-axis; dip of imbricated clasts). Here we use the extended Udden-Wentworth grain-size scale proposed by Blair & McPherson (1999) to describe the size of observed clasts, specifically the grades for 'boulders' and 'blocks' are most applicable to this study. Small boulders were measured using a tape measure, while larger boulders were measured using a TruPulse laser range finder. In addition, we used the TruPulse to survey the beach profiles and record the location of the boulders. Features characteristic of normal shallow-marine processes were recorded, if present (such as encrusting material, tilted wave-cut notches, tilted rockpools). Locations were boulders were clearly being transported down local slopes were not studied further.

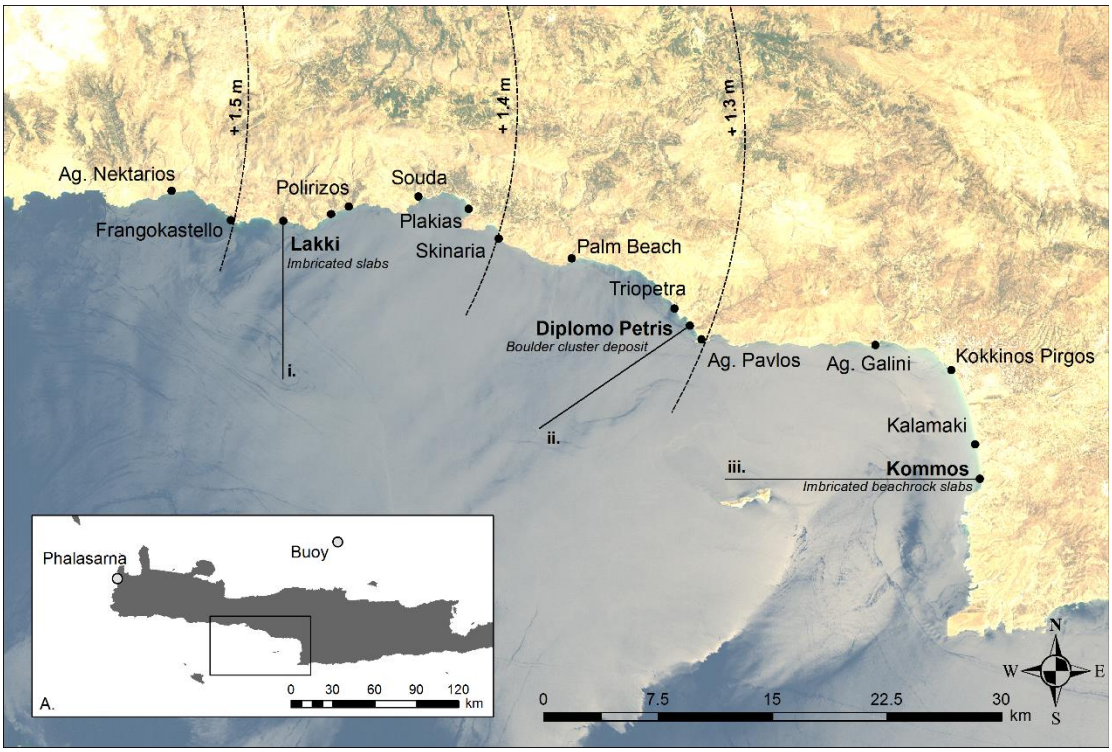

Figure 2. Landsat image of the study area (NASA Landsat Programme, 2003) showing locations visited without tsunami deposits and those with (bold) with summary of deposit in italics below, note the abbreviation Ag. for Agios. The contours of co-seismic uplift of the 365 CE event as measured in the field during this work are also indicated by dashed lines. Extent of image shown in the inset, A, with the location of the buoy used to calculate modern storm wave heights indicated.

Density of boulder lithologies were calculated in the laboratory by using the water displacement method to calculate the volume, and an electronic microbalance was used to determine the mass of boulder samples collected from each location. These data were then combined with the

measurement of the three major axes to determine the weight of the observed boulders. However, as this method approximates the boulders as cuboids the method is likely to overestimate the volume and weight of many of the boulders measured (e.g., Spiske et al., 2008; Engel & May, 2012).

Recent work by Hoffmeister *et al.* (2012) and Hoffman *et al.* (2013) have demonstrated (using a 3D terrestrial scanner) that this is indeed the case and boulder volume can be overestimated by as much as 30 – 50% resulting in an overestimate of calculated wave heights by 28 – 83%. In this study at two locations the boulders are composed of beachrock slabs that closely approximate cuboids due to their regular shape, and although some boulders possess more trapezoid and triangular shapes we focussed our measurements on the regular boulders to eliminate this bias. A similar approach was used by Lau *et al.* (2015) who studied beachrock boulder emplacement in Taiwan. Where the boulders are of variable shape and composition, we trialled a low cost technique using a 'structure from motion' (SfM) approach, this required a photographic record of the boulder (normally at least 12 photographs are needed) and the AgiSoft Photoscan software, to create detailed 3D models of several boulders from which volumes can be calculated and compared to the traditional calculations.

C-14 dating

Encrusting marine material was found to be very rare at all locations studied; however, samples of material (Serpulidae, coralline algae) were collected from all sites for AMS radiocarbon dating (Table 1). Samples were processed and analysed at the Centre for Climate, the Environment and Chronology at Queen's University Belfast. Conventional radiocarbon ages were calibrated using the MARINE13 curve in Calib 7.1 (Stuvier & Reimer, 1993; Reimer *et al*., 2013) and a marine reservoir age of $\Delta R = 65 \pm 20$.

Table 1. Radiocarbon analysis results.

Location	Sample ID	Lab ID	Material	14C age	±	1 sigma	2 sigma	Median Probability
Lakki	CR14-01	UBA-28172	Serpulid	2149	29	AD 243-350	AD 181-397	AD 293
Diplomo Petris	CR14-02	UBA-28173	Algal	2290	27	AD 73-168	AD 32-229	AD 122
Kommos	CR14-07	UBA-28174	Serpulid	Modern				
Kommos	CR14-09	UBA-28175	Serpulid	1282	36	AD 1152-1255	AD 1079-1278	AD 1192

Extreme value analysis of wave data

The Mediterranean experiences a micro-tidal regime of ~0.1-0.3 m that can easily be exceeded by storm waves. However, the southern coast of Crete is sheltered from the worst of the winter storms from the north by the mass of the island. The offshore profile of this stretch of the coast is variable with a steep offshore transition in the western part of the study area and a wide shallow foreshore in the east (Fig. 3). Therefore, the western sites are most exposed to high energy waves

than the more sheltered eastern sites. Furthermore, all areas are additionally sheltered by the presence of the island of Gavdos to the southwest. The difference in offshore topography would also result in different amounts of shoaling as waves approach the coastline.

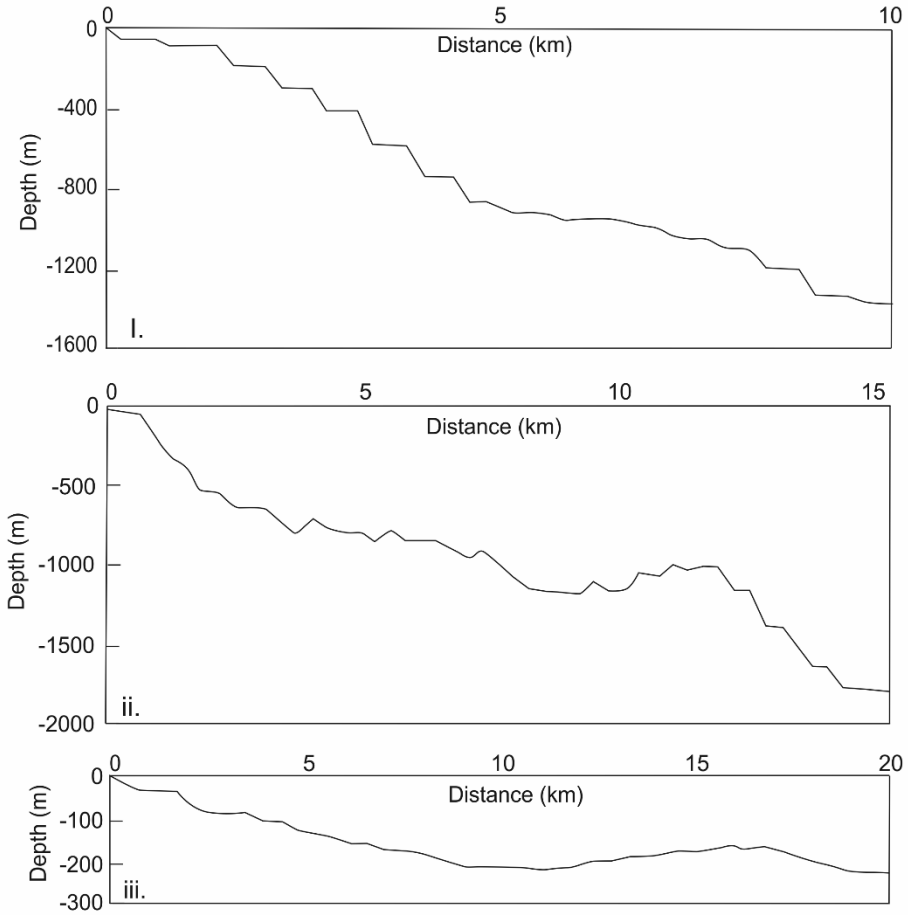

Figure 3. Bathymetric profiles (i - Lakki, ii – Diplomo Petris, iii - Kommos) taken perpendicular to the coast for each significant boulder accumulation identified, locations of these transects are shown on Figure 1. Data from EMODnet Portal for bathymetry (http://portal.emodnet-bathymetry.eu/mean-depth-full-coverage) resolution is nominally 0.125 arc-minute (~230m).

Published data suggest that waves >2.5 m rarely affect the coast with the average height of northerly waves in winter being ~1 m in height (DHI, 1971). However, in order to test these published data, we obtained annual wave data from the POSEIDON system (Table 2) from a buoy to the north of Crete (Fig. 2). Unfortunately, similar buoys are not present to the south of the island so this is the geographically closest system to the study area. To analyse the wave data return periods and to allow a comparison to be made with boulder kinematics requires the evaluation of wave height extremes; therefore, an extreme value analysis was undertaken.

Extreme Value Analysis is a statistical technique that is based on an understanding of the probability of a series of observed data, which can allow extrapolation to evaluate the unseen highs and lows (extremes) of the data. There are a variety of techniques available to undertake an Extreme Value Analysis (see Coles, 2001), with the most common technique being the Generalised Extreme Value (GEV) distribution. However, for a temporally short data set there are several drawbacks with the GEV in that it requires typically > 20 years of data (Tawn & Vassie, 1990; Coles, 2001; Whitworth, 2015).

To combat the limitations of the GEV, the r-largest approach was developed by Smith (1986), so that temporally shorter datasets could be analysed. In an extension to the Generalised Extreme Value Distribution, the r-largest values for each year, $z = (z^{(1)}, \ldots, z^{(r)})$ where $r \geq 1$, are extracted from each year's data and ordered. The joint probability density function is then of the form:

$$f(z) = \exp[-\{1+\xi(\frac{x^{(r)}-\mu}{\sigma})\}^{-\frac{1}{\xi}}]\prod_{k=1}^{r}\frac{1}{\sigma}\{1+\xi(\frac{x^{(k)}-\mu}{\sigma})\}^{-\frac{1}{\xi}-1} \quad (1)$$

The three parameters (μ, σ, ξ) correspond to the parameters of the GEV model (Butler *et al*., 2007).

To undertake the r-largest analysis, the 10 (r) largest observed maxima for each year of the data set were compiled in an excel spreadsheet and then converted into a text file. The text file was then imported into a software package called "Extremes" (Gilland & Katz, 2006). The value of r (2 to 10) was then varied to identify the value of r that provided the best fit to the data by evaluating the various plots. The software was then interrogated to evaluate the precise return level and return period with the required confidence limits (Fig. 4).

Table 2. Ten largest independent annual wave heights recorded for the period 2000 to 2006. This data is used as part of the R largest extreme value analysis of the data.

Year	R1	R2	R3	R4	R5	R6	R7	R8	R9	R10
2000	3.87	2.99	2.99	2.98	2.89	2.87	2.86	2.85	2.83	2.80
2001	4.78	4.60	3.83	3.79	3.77	3.55	3.52	3.44	3.41	3.20
2002	4.65	4.61	4.43	4.17	4.15	4.07	4.04	3.83	3.53	3.05
2003	5.43	5.23	4.83	4.02	3.88	3.58	3.16	3.14	3.13	3.09
2004	4.97	4.44	4.18	4.09	4.04	3.96	3.47	3.47	3.33	3.31
2005	4.17	3.53	3.38	3.30	3.06	2.92	2.90	2.85	2.84	2.80
2006	3.90	3.65	3.62	3.43	3.17	3.07	3.01	2.92	2.91	2.78

Figure 4 shows that for a 1 in 100 return period maximum wave height could be the order of 5.5 m based on extreme value analysis (R largest) of 7 years data (2000 – 2006). We therefore consider that this is the maximum storm wave height that could affect the more sheltered southern coast.

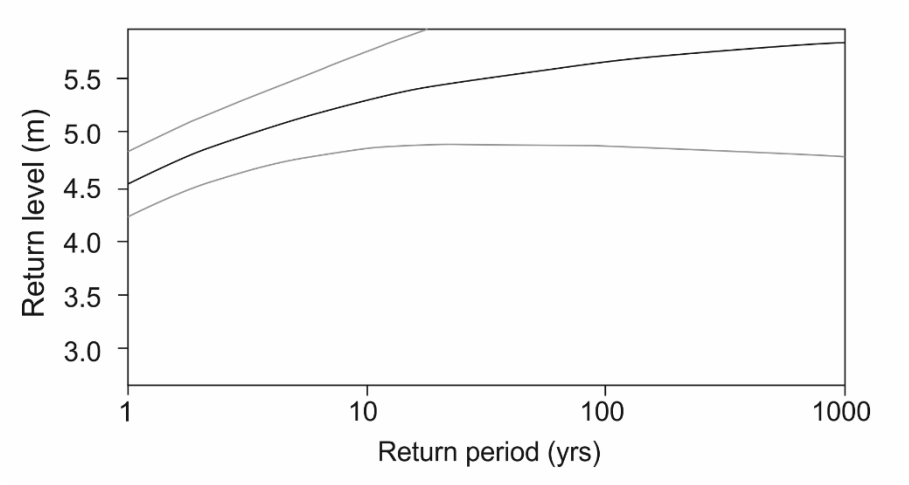

Figure 4. Wave height return period plot based on a R largest extreme value analysis of the data presented in Table 1. The black line indicates the prediction and the grey lines show the 95% confidence limits.

Hydrodynamic Equations

Hydrodynamic equations for storm and tsunamis were initially derived by Nott (1997, 2003a, b) to estimate the minimum wave height and velocity needed to initiate boulder transport located in three environments; submerged, subaerial and joint bounded blocks. These original equations have subsequently been improved to increase accuracy and include variables for the processes of dislodgement, emplacement and transport style (sliding, rolling, saltation) as well as the effect of slope at the pre-transport location (Noormets *et al*., 2004; Imamura *et al*., 2008; Pignatelli *et al*., 2009; Benner *et al*., 2010; Nandasena *et al*., 2011).

To calculate the flow velocity required to initiate clast transport, the equations of Nandasena *et al*. (2011) were used (Appendix A, equations. 1-4). As the transportation mechanisms and exact initial location (submerged, subaerial, joint-bounded) of all boulders cannot be determined a range of values were calculated for each boulder where appropriate (Table 3). In order to quantify the potential storm (H_s) or tsunami (H_t) wave height required to the displace the boulders the hydrodynamic approach of Benner *et al*. (2010) was used for a submerged pre-transport scenario and the equations of Pignatelli *et al*. (2009) were used for the joint-bounded boulder scenario (Appendix A, equations 5-8), we also use the modified Nott equations proposed by Barbano *et al*., (2010) in comparison (Appendix A; equations 9-14).

Table 3 (next page). Location, size (maximum length of the three major axes) and weight of boulders measured along the Cretan coast, velocities required to initiate transport are derived from the equations of Nandasena et al. (2011) and the tsunami (Ht) and storm wave (Hs) heights required for their transport are found using the equations of Pignatelli et al., (2009); Benner et al., (2010) and Barbano et al., (2010). SM – submerged; SA – subaerial; JB – joint bounded.

		Boulder axes (m)						Nandansena et al. (2011)				Pignatelli et al. (2009) JB		Benner et al. (2010)		Barbano et al. (2010)					
Location	Boulder	A	B	C	Volume (m^3)	Mass (kg)	Mass (T)	SM Sliding (ms^{-1})	SM Rolling (ms^{-1})	SA (ms^{-1})	JB (ms^{-1})	Ht (m)	Hs (m)	SM - Ht (m)	SM - Hs (m)	SM Ht (m)	SM Hs (m)	SA Ht (m)	SA Hs (m)	JB Ht (m)	JB Hs (m)
	B	2.17	1.41	0.20	0.61	1761	1.8	1.94	0.45	0.68	20.41	0.81	4.22					0.91	3.66	1.05	4.22
Lakki	C	2.82	2.10	0.34	2.01	5793	5.8	2.53	0.79	0.71	23.27	1.38	7.18					1.50	5.99	1.79	7.17
	14a	0.79	0.80	0.40	0.25	727	0.7	2.69	2.26	1.96	12.32	1.62	8.45					0.74	2.97	2.11	8.44
	1	7.80	3.30	3.20	82.37	256988	257.0	8.42	9.97	9.49				2.20	8.79	2.79	9.14	2.35	9.42		
	2	3.00	2.10	1.80	11.34	35381	35.4	6.68	8.30	7.94				1.56	6.25	1.97	6.17	1.65	6.61		
	3	1.50	1.10	1.00	1.65	5148	5.1	4.85	5.89	5.62				0.78	3.11	0.98	3.15	0.83	3.31		
	4	2.40	1.65	1.50	5.94	18533	18.5	5.94	7.21	6.88				1.17	4.66	1.47	4.72	1.24	4.96		
	5	4.65	2.10	1.60	15.62	48747	48.7	6.63	8.61	8.28				1.72	6.88	2.16	6.45	1.80	7.19		
	6	5.00	5.00	4.20	105.00	327600	327.6	10.29	12.89	12.35				3.79	15.14	4.76	14.81	3.99	15.97		
	7	4.50	4.60	3.10	64.17	200210	200.2	9.74	13.17	12.73				4.12	16.49	5.18	14.59	4.25	17.00		
	8	2.70	4.30	2.80	32.51	101425	101.4	9.39	12.84	12.43				3.94	15.77	4.96	13.73	4.05	16.20		
	10	3.00	1.80	1.40	7.56	23587	23.6	6.15	7.92	7.61				1.45	5.81	1.82	5.49	1.52	6.08		
	12	2.10	2.60	2.10	11.47	35774	35.8	7.40	9.41	9.03				2.03	8.14	2.55	7.82	2.14	8.55		
Diplomo Petris	13	3.10	1.80	1.40	7.81	24373	24.4	6.15	7.92	7.61				1.45	5.81	1.82	5.49	1.52	6.08		
	14	2.80	1.80	1.20	6.05	18870	18.9	6.09	8.26	7.99				1.63	6.50	2.04	5.72	1.67	6.69		
	15	1.40	1.30	1.00	1.82	5678	5.7	5.22	6.75	6.49				1.06	4.23	1.33	3.98	1.11	4.42		
	20	6.00	4.50	3.50	94.50	294840	294.8	9.72	12.52	12.04				3.63	14.52	4.55	13.72	3.80	15.19		
	21	2.50	1.60	1.50	6.00	18720	18.7	5.85	7.03	6.70				1.10	4.40	1.39	4.51	1.17	4.69		
	22	2.50	1.50	1.10	4.13	12870	12.9	5.59	7.35	7.09				1.27	5.06	1.59	4.66	1.32	5.27		
	22a	2.20	1.50	1.40	4.62	14414	14.4	5.67	6.81	6.49				1.04	4.14	1.31	4.24	1.10	4.42		
	23	12.00	4.50	4.10	221.40	690768	690.8	9.80	11.90	11.36				3.17	12.70	4.00	12.86	3.38	13.51		
	24	1.20	1.60	1.00	1.92	5990	6.0	5.71	7.91	7.66				1.51	6.02	1.90	5.14	1.54	6.16		
	27	1.30	1.30	0.90	1.52	4746	4.7	5.19	6.95	6.71				1.14	4.57	1.44	4.10	1.18	4.73		
	31	3.60	3.40	3.40	41.62	129842	129.8		10.01	9.51				2.20	8.80	2.80	9.26	2.36	9.46		
	32	3.00	2.20	1.50	9.90	30888	30.9		9.08	8.77				1.96	7.82	2.46	6.96	2.02	8.08		
	33	1.70	1.30	1.20	2.65	8274	8.3		6.37	6.07				0.91	3.63	1.14	3.69	0.97	3.86		
Kommos	1	2.50	1.40	0.25	0.88	1893	1.9	3.00	4.66	4.57	5.06	0.35	2.84	0.63	2.09	1.14	1.47	0.65	2.60	0.80	3.19

2	1.50	1.00	0.15	0.23	487	0.5	2.45	3.71	3.65	3.92	0.21	1.70	0.40	1.32	0.75	0.91	0.41	1.66	0.48	1.91
3	1.80	0.90	0.18	0.29	631	0.6	2.45	3.87	3.78	4.29	0.26	2.04	0.43	1.44	0.76	1.04	0.45	1.79	0.57	2.30
4	2.00	1.90	0.18	0.68	1480	1.5	3.03	4.24	4.20	4.29	0.26	2.04	0.52	1.72	1.05	1.14	0.55	2.18	0.57	2.30
5	2.20	1.10	0.20	0.48	1047	1.0	2.67	4.16	4.07	4.52	0.28	2.27	0.50	1.66	0.90	1.18	0.52	2.07	0.64	2.55
6	1.70	1.50	0.35	0.89	1931	1.9	3.25	5.19	5.06	5.98	0.50	3.97	0.77	2.60	1.32	1.93	0.80	3.21	1.12	4.47
7	1.15	0.95	0.15	0.16	355	0.4	2.41	3.68	3.62	3.92	0.21	1.70	0.39	1.30	0.73	0.90	0.41	1.63	0.48	1.91
8	1.40	1.20	0.20	0.34	727	0.7	2.74	4.22	4.14	4.52	0.28	2.27	0.51	1.71	0.95	1.19	0.53	2.14	0.64	2.55
9	1.00	0.45	0.20	0.09	195	0.2	1.92	2.99	2.84	4.52	0.28	2.27	0.25	0.87	0.36	0.78	0.26	1.03	0.64	2.55
10	2.15	1.50	0.20	0.65	1396	1.4	2.93	4.35	4.29	4.52	0.28	2.27	0.55	1.81	1.05	1.23	0.57	2.28	0.64	2.55
11	3.15	0.90	0.42	1.19	2576	2.6	1.93	4.20	3.98	6.56	0.60	4.77	0.49	1.73	0.70	1.58	0.51	2.04	1.34	5.36
12	1.40	1.05	0.19	0.28	604	0.6	2.60	4.05	3.97	4.41	0.27	2.16	0.47	1.58	0.86	1.12	0.49	1.97	0.61	2.43
13	1.10	1.04	0.12	0.14	297	0.3	2.36	3.42	3.37	3.50	0.17	1.36	0.34	1.12	0.66	0.75	0.35	1.41	0.38	1.53
14	1.54	0.95	0.18	0.26	570	0.6	4.20	3.91	3.83	4.29	0.26	2.04	0.44	1.47	0.79	1.05	0.46	1.83	0.57	2.30
15	2.52	1.77	0.14	0.62	1351	1.4	2.79	3.78	3.75	3.79	0.20	1.59	0.42	1.37	0.84	0.90	0.43	1.73	0.45	1.79
16	1.40	1.13	0.13	0.21	445	0.4	2.46	3.56	3.51	3.65	0.18	1.48	0.37	1.21	0.72	0.81	0.38	1.53	0.41	1.66
17	1.66	1.50	0.23	0.57	1239	1.2	3.01	4.58	4.51	4.85	0.33	2.61	0.61	2.02	1.14	1.39	0.63	2.52	0.73	2.94
18	2.05	1.62	0.20	0.66	1437	1.4	2.99	4.38	4.33	4.52	0.28	2.27	0.56	1.84	1.08	1.24	0.58	2.32	0.64	2.55

Observations

Field evidence from Lakki

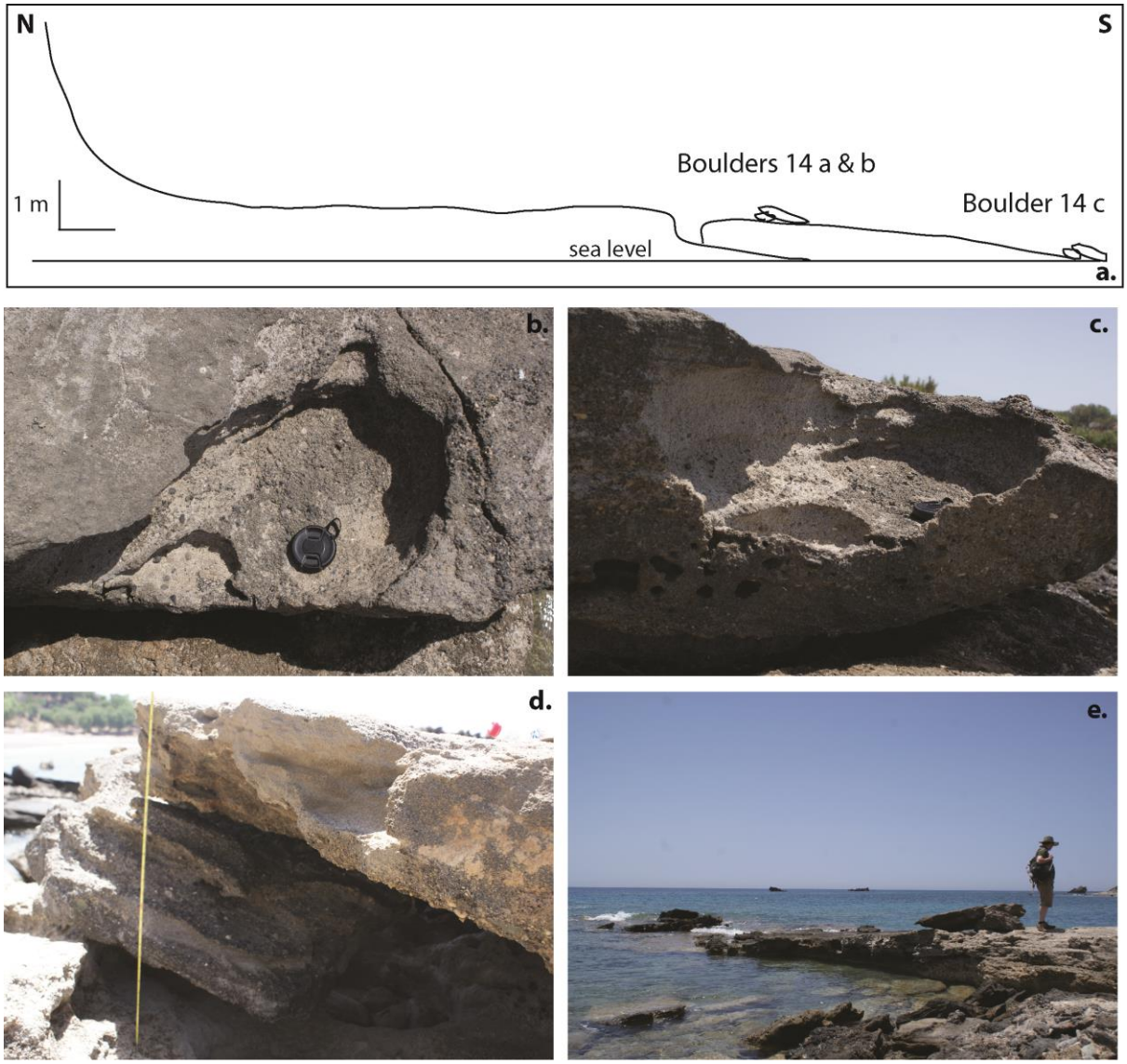

Figure 5. Photographs of the Lakki site: a) sketch profile of the beach showing location of boulders; b) plan view and c) side view of inset rock pools showing evidence for movement of the boulder 14 b (lens cap for scale); d) photograph of the imbricated nature of the boulders 14 a and b (tape measure 1 m) and e) general view of the location.

Lakki (35.18° N 24.27° E) is a small embayment ~ 350 m long near Frangokastello (Fig. 2). Here, the low cliffs are formed from Neogene cream-coloured bioclastic sandy limestone with unconformably overlying dark grey, coarse-grained litharenites from Quaternary alluvial fans (Pope *et al*., 2008). In the centre of the bay a linear exposure of the bioclastic limestone extends ~ 20 m into the sea, with the upper surface 1.35 ± 0.5 m above present sea-level dipping seawards at ~ 3° (Fig. 5). Wave formed pools have developed in the upper surface of the rocky exposure. Several large tabular, coarse – very coarse boulders of litharenite are emplaced on top of one another on this exposure

dipping seawards (174° - 214°) with slight imbrication (Fig. 5). Other slabs are observed adjacent to the outcrop but it is unclear if the placement of these blocks has been altered by recent development of the area. Of note is boulder 'b', on the upper surface the boulder has a karstic pool, which shows evidence of reworking in the intertidal zone due to the base of the pool having been tilted from horizontal and then further erosion forming the present horizontal pool (Fig. 5). On the base of this boulder were a mass of encrusting serpulid worm tubes, sample CR14-01 was sampled from here giving a conventional radiocarbon age of 2149 ± 29 yrs BP, which equates to a 2 σ calibrated date of 181 – 397 CE (Table 2). Boulder c is also interesting as it is broken into two parts, presumably upon placement in its current position, which may suggest transport through saltation rather than sliding or rolling.

The density of the litharenite was determined as 2.88 g/cm^3, thus the largest boulder with a long axis > 2.8 m (Table 4) has a mass of ~5.8 tonnes. Hydrodynamic calculations (Benner *et al*., 2010) indicate that the minimum wave height needed to move this slab, assuming a sub-aerial origin (as indicated by the tilted pool), is 3.2 m for a storm and 0.15 m for a tsunami. By contrast, Pignatelli *et al*.'s (2009) equations for a joint bounded block scenario suggests a minimum H_s = 8.4 m and H_t =1.6 m. Flow velocity can also be calculated for submerged, subaerial block and joint bounded transport (Nandasena *et al*., 2011), which suggests that the minimum flow velocities of 0.1-4.5 ms^{-1} are required to initiate the transport of these blocks. Although this value is considerably higher if a joint-bounded block scenario is considered, in this case a flow velocity of > 12 ms^{-1} would be required.

Field evidence from Diplomo Petris

South of the small village of Triopetra is a sheltered 1km stretch of sandy beach (Diplomo Petris; 35.11° N 24.555° E) where bedded beachrock is exposed along much of the beach outcropping partly below and partly above present sea-level dipping shallowly seaward (≤ 10°) and is currently being eroded by wave action. To the north the beach is backed by low cliffs of Upper Miocene marl and sandy limestones (Tortorici et al., 2012), with a discontinuous raised marine shoreline composed of cobbles at ~ 5 m absl. Heading southwards the cliffs come closer to the beach and bedrock outcrops form a small headland. The bedrock is formed of steeply dipping and fractured dark grey to brown litharenite characteristic of the lower unit of the Cretan ophiolitic nappe, probably of Paleocene age (Tortorici et al., 2012). The boundary between the Paleogene and Neogene rocks is poorly exposed but appears to be a thin sliver (< 100 m thick) of tectonic melange. To the south of this bedrock exposure is the mouth of a river, which dominantly drains flysch and limestone bedrock.

At the headland (Table 4; Figs. 2 & 6) a cluster of fine boulders to fine blocks is observed cemented into the beachrock at the shoreline. The clasts are of mixed lithologies with limestone, quartzite and litharenite being the most common but boulders of sheared metamorphics, red sandstone and green conglomerate are also present. While the litharenites, metamorphic rocks and other exotic boulders were probably derived from the adjacent cliffs, the limestone boulders are typical of the Pindos and Tripolitiza units that do not outcrop in this location nor were these lithologies observable in the melange, indicating that these large blocks are not derived from the adjacent cliff.

The lithology of the boulders could be consistent with them having been transported downstream in the river system. However, several lines of evidence suggest that this is unlikely. Firstly and perhaps most compellingly, is the presence of a wave cut or tidal notch on a number of the limestone boulders (Fig. 6c). Observation of the notch shows that it is remarkably similar to that preserved *in situ* elsewhere and uplifted by the 365 CE earthquake (i.e., Pirazzoli *et al*., 1992; Shaw *et al*., 2008), and is further evidence that the boulders are not the result of recent cliff collapse.

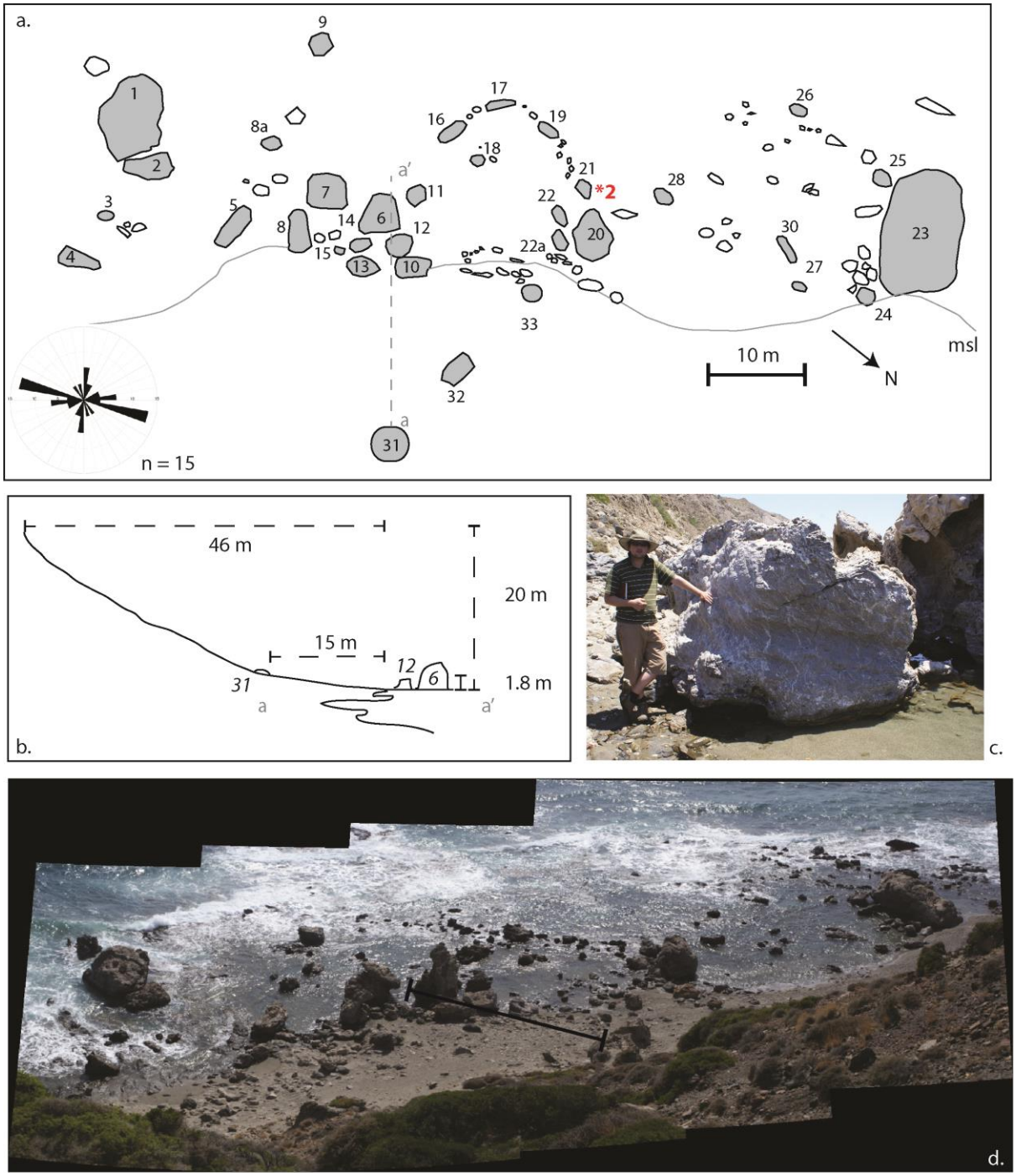

*Figure 6. Photographs and maps of Diplomo Petris; a) map of the boulder deposit with inset rose diagram showing orientation of the long axes of boulders; *2 indicates the location of radiocarbon sample CR14-02; b) sketch profile of the beach section along the line a-a'; c) photograph of boulder 12 showing tilted wave cut notch; d) panoramic view of the boulder deposits from the cliff top with line of transect shown.*

Sample CR14-02 was taken from the bioencrustation associated with the notch observed on boulder 21 (Fig. 7b), this returned a conventional radiocarbon date of 2290 ± 27 yrs BP (calibrated 2σ age 23 – 229 CE; Table 2) consistent with this interpretation. The notch is observed to be orientated either horizontally or tilted at up to 12° and it is observed to lie across a range of elevations from 0.4 to 0.9 m absl. By contrast, our measurements indicate that the 365 CE uplift in this location should result in a notch apex at ~ 1.3 m in elevation (Fig. 2). The presence of different notch heights, heights

lower than the predicted elevation for an uplifted notch, and the different orientations of the notches strongly indicate that these boulders have been reworked within the intertidal zone after notch formation. Additionally, Lithophagid borings are visible on the side of many of the boulders and blocks above present sea level (Fig. 7a), further evidence of previous submergence. Secondly, the largest of the blocks weighs in excess of 690 tonnes (longest axis 12 m, intermediate axis 4.5 m) with many blocks weighing > 20 tonnes (Table 4). Observations of the modern bedload of the river show that these boulders are significantly larger than the cobbles transported at the present time. Furthermore, the boulder cluster is not located at the mouth of the river but 100 m north, although some of the smaller clasts could, and probably have been reworked locally by waves, longshore drift is expected to be directed to the southeast as this is the direction of the prevailing winds (Cavaleri & Sclavo, 2006). It is possible that the largest limestone boulders have been transported from Agios Pavlos, the closest coastal limestone outcrop with clear tidal notches, located ~1 km to the south (Fig. 2).

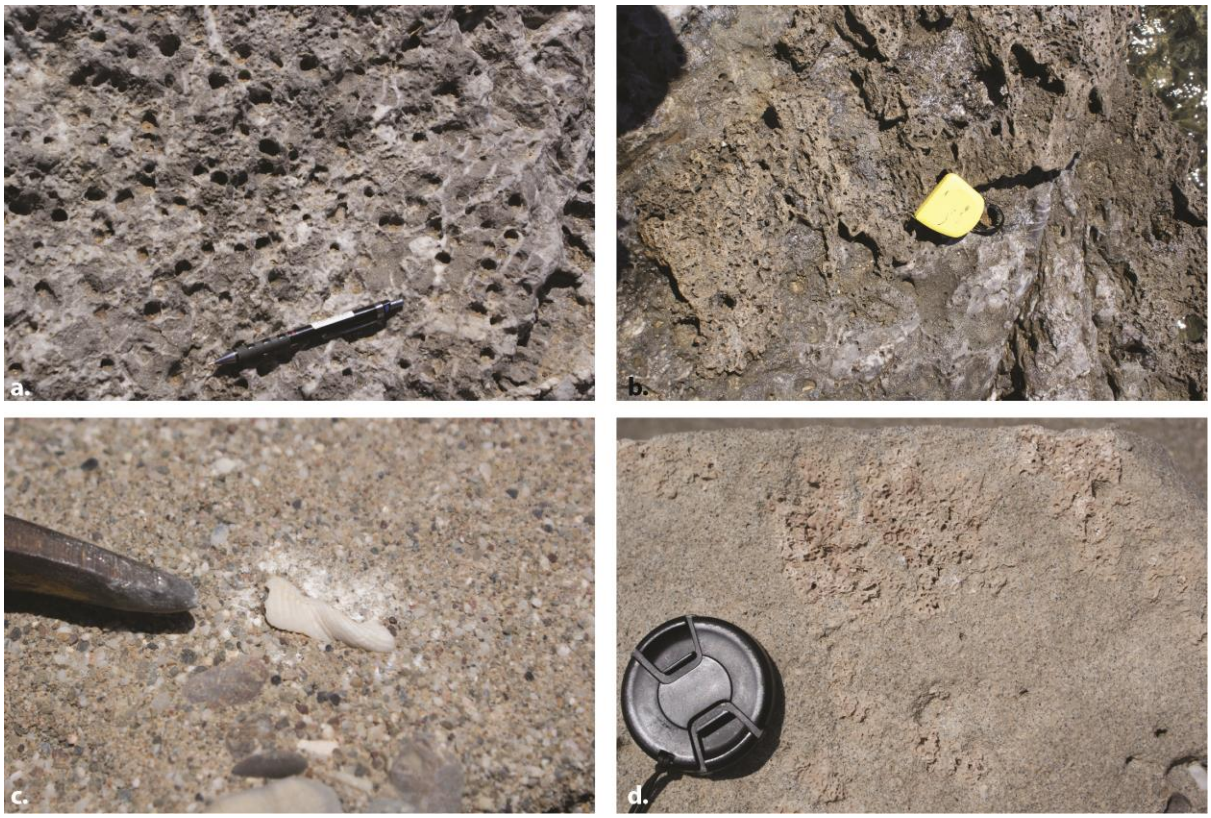

Figure 7. Photograph of Lithophagid type borings observed at Diplomo Petris (pencil for scale); b) Algal bioencrustation sampled for C-14 dating at Diplomo Petris (tape measure for scale); c) example of bivalve material embedded within the beachrock at Kommos indicating marine origin of the litharenite (tip of hammer for scale); d) encrusting serpulid material on a beach rock from Kommos sampled for c-14 dating (lens cap for scale).

The limestone boulders are generally tabular to sub-spherical, sub-angular in shape and moderately weathered, with joint or fractures related to *in situ* deformation not later fracturing. Two samples of limestone were collected for density analysis and give an average density of 3.12 g/cm^3, consistent with the recrystallized nature of the limestone. Owing to the position in the intertidal zone some boulders were inaccessible due to excessive water depth and/or the presence of a deep pool surrounding the boulders. As a result the maximum axes of 23 boulders were measured but the location of 12 other boulders with an intermediate axis >0.5 m were also recorded (Fig. 6). Fine

boulders and smaller were not measured as it is likely that these can be reworked during winter storms. In addition, the orientation of the long axis of the boulders was recorded.

The largest block (No 23; Fig. 6) weighs ~ 690 tonnes, there are another 5 boulders and fine blocks with a mass exceeding 100 tonnes (Table 3). Block No. 23 would require a storm wave of ~15 m high to initiate transport and a tsunami wave of <4.5 m high. The presence of the raised tidal notch; however, strongly suggests a sub-aerial origin for the blocks and boulders resulting in slightly lower predicted wave heights (H_s = 12.7 m; H_t = 3.2 m). Current velocity calculations indicate that for a sub-aerial origin a current of velocity of 12 ms^{-1} is required to initiate boulder transport. Boulder long axes are generally orientated ~ E – W but there is a subset of boulders that are orientated N – S (Fig. 6a).

Tsunami field evidence from Kommos

Kommos (35.01°N, 24.76°E) on the southern edge of the Mesaras Plain is the end of a long sandy beach running for many kilometres (Fig. 8). Uplift from the 365 CE earthquake is negligible this far to the east (Pirazzoli *et al*., 1992) and the ruins of the Minoan-aged port of Kommos are located behind the recent dunes. At two locations along this stretch of beach, dislocated and imbricated medium to coarse-grained beachrock boulders (Fig. 7c), with a slab morphology are present ~ 20 m inland and 1.5 – 2 m absl. *In situ* beachrock is exposed, as at Diplomo Petris, above and below present sea-level, dipping shallowly seaward.

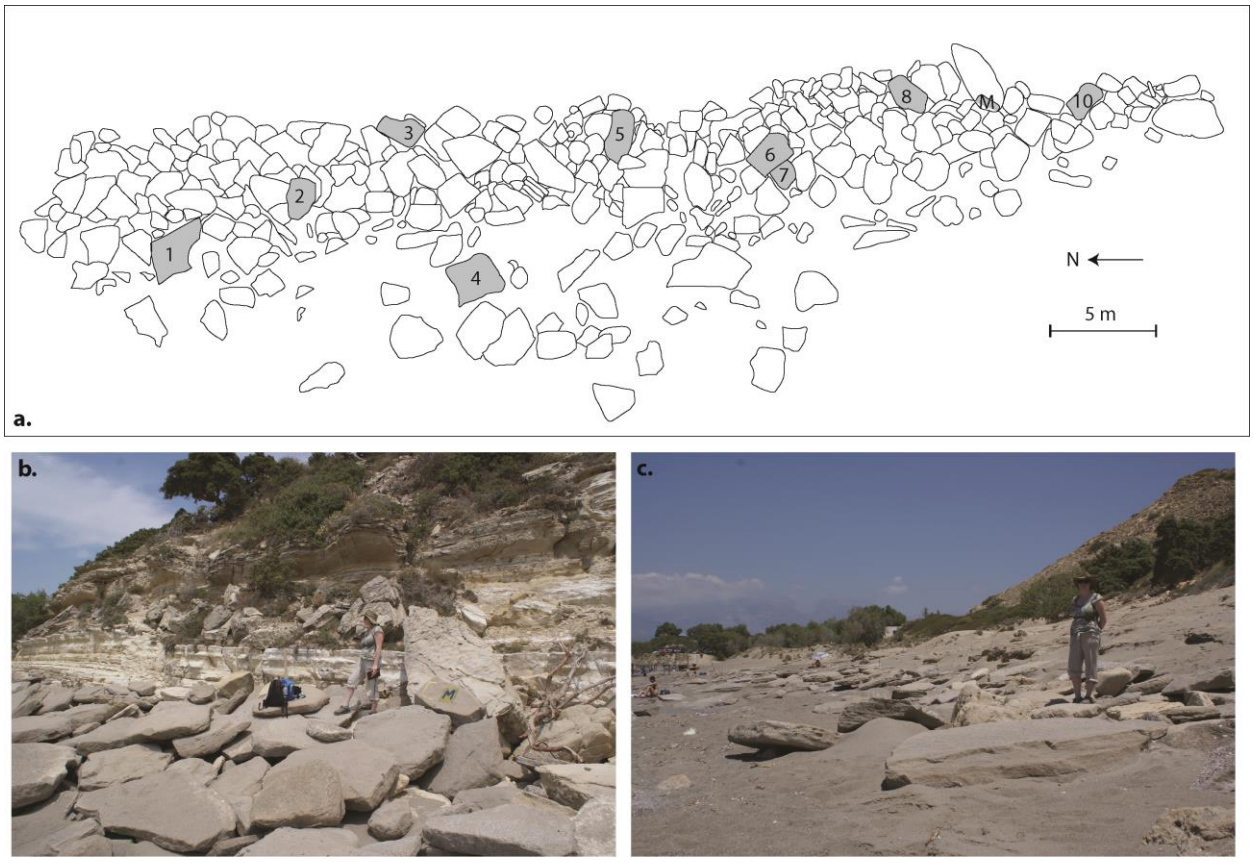

Figure 8. Photographs and maps of Kommos; a) sketch map of boulder deposit located at the foot of a small cliff, with measured boulders indicated in grey with number; b) photograph of the boulders shown in a.; c) photograph of the boulders further to the south prior to redevelopment.

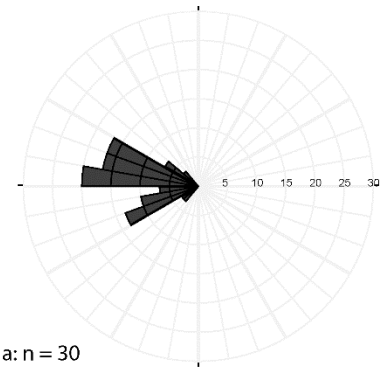

a: n = 30

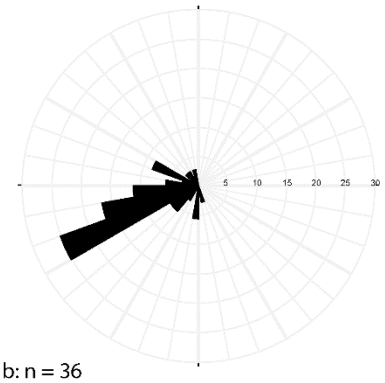

b: n = 36

Figure 9. Rose diagrams showing the dip directions of beachrocks slabs measured at the two locations at Kommos (Fig. 2). A. Measurements taken at UTM zone 35°S 0295620/3876465 (Fig. 8c); B. Measurements taken at UTM zone 35°S 0295639/3876960 (Fig. 8b).

At the first location, the beachrock slabs dipped to the west (seawards; Fig. 9a), have a tabular shape with the a- and b-axes typically 1 – 3 m long and the c-axis ≤ 0.2 m (Table 4) and were partly covered by dune sands. Unfortunately, when we returned to this location to undertake further field data collection we discovered that the blocks had been bulldozed from their previous locations in order to develop the beach amenities – this prevented further meaningful data collection.

At the second location, 500 m to the north, the beachrock slabs are very similar in composition, size and morphology, although the dip is more variable (Fig. 9b) likely due to their location at the foot of a small cliff of Messinian cream-coloured marl (ten Veen & Kleinspehn, 2003). The bedrock marls are lithologically distinct to the beachrock forming the displaced blocks, and although boulders of marl are present at the base of the cliff these were not subsequently measured.

Several beachrock slabs at Kommos were observed to have encrusting Serpulid worms tubes on the surface, which were sampled for radiocarbon dating (Fig. 7d). Two samples were submitted for dating, one returned a modern age while the other gave a calibrated age of 1152 – 1255 CE (Table 1). Given the location of the boulders above high tide this modern age implies that this boulder has been recently transported onshore.

The size and shape of the beachrock boulders is fairly tightly grouped with long axes typically in the range of 2.5 – 1 m and a thickness of ~0.2 m. The beachrock is porous so a wet density was calculated at 2.16 g/cm^3 (dry density = 2.0 g/cm^3) resulting in the majority of the larger slabs having a mass in the order of 1 – 2.5 tonnes. Given that beachrock can be observed *in situ* in the intertidal zone at the present day, it is probable that these blocks have been reworked from a joint-bounded location. To emplace these boulders onto the shore a maximum H_s of 5 m and a H_t of 1.5 m is needed with a flow velocity of ≤ 6.5 ms^{-1} (Table 4).

Photographic Analysis of blocks

Recent work by Hoffmeister *et al.* (2012) and Hoffman *et al.* (2013) demonstrated that approximating the volume irregular boulders as cuboids often results in the overestimation of the boulder mass and therefore, the results of the hydrodynamic equations. Hoffman *et al.* (2013) measured three boulders in Oman, and found that the high precision lidar scans resulted in volumes ~30-40 % lower than the volume derived by multiplying the 3-axes of the boulders. Using a similar method Hoffmeister *et al.* (2012) investigated sites in western Greece, demonstrating that lidar scans resulted in volume differences of up to 70 %. In each case this would indicate that the results from the hydrodynamic equations would overestimate the tsunami wave height and velocities needed to move the tsunami blocks and boulders.

At Lakki and Kommos the boulders investigated are tabular in shape and therefore, are close to the ideal cuboid. Therefore, the simple mass approximation should be accurate for calculating volume and resultant hydrological parameters. However at Diplomo Petris, some of the boulders are highly irregular in shape. In order to assess the accuracy of our measurements we constructed 3D models using a structure from motion approach (SfM) of three boulders that had 360° accessibility (Fig. 10). The process is straightforward in that a series of scaled photographs (> 12) are taken around the boulder in question. We then used the Agisoft Photoscan software package to generate a 3D model of each boulder and calculate a volume to compare with the volume calculated from field measurements of the major axes (Table 4).

Our photogrammetric analysis indicates that the volumes of boulders 4 and 10 are significantly overestimated (Table 4) if the traditional method is applied supporting the previous analyses of Hoffmeister *et al.* (2012) and Hoffman *et al.* (2013). However, the volume of boulder 32 is underestimated using the traditional method compared to the 3D photogrammetric analysis. This result reflects that boulders 4 and 10 diverge from an ideal cuboid by a significant degree, whereas boulder 32 is a more regular shape, as are the majority of the largest boulders surveyed. Therefore, although we recognise that the calculated values for some of the small boulders will be significantly overestimated, this method indicates that for the more cuboid boulders measuring the major axes can result in reliable data. This photogrammetric method also is a low cost option for the assessment of boulder volume, in comparison to Lidar based systems, and so offers high potential for future studies.

Table 4. Comparison of boulder volumes derived by different techniques.

Boulder No	Volume from 3D model(m^3)	Volume from field measurement	Ratio est. volume to 3D volume (%)
4	2.48	5.94	239.5
10	2.95	7.56	256.3
32	10.72	9.9	92.4

Discussion - Storm or tsunami deposit?

By considering the field observations and the wave heights estimated from the hydrodynamic models it is now possible to make an assessment of which, if any of the boulder clusters identified may have been deposited by tsunamis. The evidence is most ambiguous at Kommos. The imbrication direction combined with a near shore origin for these boulders is strongly indicative of emplacement by extreme waves. Yet imbrication has been identified in both storm and tsunami boulder deposits and therefore is not discriminatory (Paris *et al*., 2009; Etienne & Paris, 2010; Goto *et al*., 2012). Given that beachrock is exposed at sea level, it is likely that an event not only transported the slabs to the current position but also plucked them from an *in situ* location. Therefore, the joint bounded scenario was used for the calculation of extreme waves. Many of the boulders only weigh ~ 1 tonne, thus storm waves of ≤ 5.5 m would be needed to move the largest from a sub-aerial position when applying the equations of Barbano et al. (2010). By contrast, a tsunami would need to be only 1.3 m high to initiate transport. These values are reduced by ~ 10 % when Pignatelli et al.'s (2009) equations are used. Therefore, transport and deposition by a large storm cannot be ruled out at this

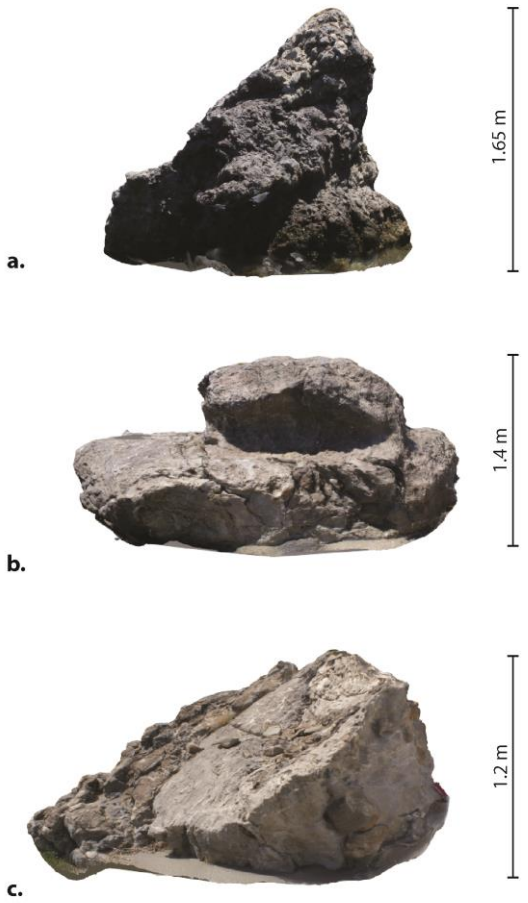

Figure 10. Photogrammetric 3D models of boulders 4, 10 and 32 from Diplomo Petris (Fig. 6a).

location as although 5 m high storm waves are rare, they are possible in the Mediterranean based upon extreme value analysis. In addition, velocities for the initiation of transportation fall in the range of 3 – 6 ms^{-1} depending on the equation used. These values are well within the tolerance for a large storm, where wave velocities of up to 8 ms^{-1} in coastal settings have been recorded (Dally, 2005; EurOtop, 2007). Furthermore, the boulders form a beach parallel ridge rather than a distributed field, more characteristic of storms than tsunamis. This interpretation of a storm deposition is supported by the dating that returned a modern date for one of the samples suggesting recent removal from the intertidal zone. Although, the other sample gives a much older date of 1192 CE, which would not be inconsistent with the 1303 CE tsunami (Guidoboni & Comastri, 1997) the evidence is not compelling. Therefore, all things considered, the boulder deposit observed at Kommos cannot be confidently ascribed to a tsunami as it equally could be the result of storm deposition.

Further north at Lakki, a small number of blocks were observed lying on top of a raised platform. This part of the coast was uplifted by 1.7 – 2.0 m in 365 CE, greater than the height of the surface upon which the slabs rest, indicating that the platform was below sea level prior to that time. Again, these slabs show evidence for reworking in the intertidal zone due to the presence of a tilted tidal pool, suggesting reworking from an originally sub-aerial location or possibly a sub-aerial joint bounded position. For the blocks to be transported a storm wave of 6.0 – 8.5 m high would be required. Current velocities for a subaerial origin are modest ($\leq$ 5 ms^{-1}) but much higher if a joint-bounded origin is considered (23 ms^{-1}). These values are at the extreme for that expected within the Mediterranean, as especially as the location is somewhat sheltered within a small bay, and exceed values derived from the extreme value analysis. Therefore, on balance it is slightly more likely that these blocks may have been transported by a tsunami wave ~2 m high but the sedimentological evidence is equivocal. However, the calibrated radiocarbon age of 293 CE is consistent with reworking by the 365 CE tsunami.

The final location of Diplomo Petris has the most convincing evidence for block transport by tsunamis. Wave height calculations indicate that storm waves of > 14 - 16 m and current velocities of > 13 ms^{-1} would be needed to move these boulders considering a submerged position. Furthermore, as indicated by bioerosional notches part way up the boulders, as subaerial origin is more likely for the boulder origin increasing the required storm wave heights to 17 m. These values far exceed the possible storm wave height along this part of the Cretan coast.

However, a tsunami wave of 4-5 m high could transport blocks of this size and morphology, and the calculated velocities are consistent with observations of recent tsunamis, which indicate

tsunami wave velocities of 10 – 20 ms^{-1} (Titov & Synolakis, 1997; Phuwieng *et al*., 2008). The presence of tidal notches (dated to 365 CE by Shaw *et al*., (2008) and our sample) also indicates that these boulders were present at sea-level prior to the 365 CE uplift and were subsequently dislocated from their original position, most likely by this catastrophic event. A tsunami origin is also supported by the scattered and distributed debris field with no trend in clast size distribution.

Measurements of other tsunami boulder deposits indicate that the long axis of the boulders is typically oriented perpendicular to the flow direction (i.e., Goto et al., 2007; Etienne et al., 2011; Richmond et al., 2011). In this case that would suggest flow from the south, as boulders are orientated ~ E-W (Fig. 6a), consistent with the closest exposure of Mesozoic limestones (forming the largest of the boulders) at Agios Pavlos. This direction is similar to the NE direction of flow generally inferred from tsunami models of the event (i.e., Shaw *et al*., 2008; England *et al*., 2015). Furthermore, the calculated wave heights are comparable with predicted values from tsunami models of this event (Shaw *et al*., 2008; England *et al*., 2015). Therefore, on balance, we interpret these boulders to have been emplaced by a significant tsunami, probably the 365 CE tsunami.

Conclusions

At three locations (Lakki, Kommos and Diplomo Petris) on the coast of Crete bolder deposits were investigated in order to determine the mechanism for emplacement. At Lakki and Kommos the boulders are tabular in shape and formed of local alluvial fan material and beachrock, respectively. The size of the slabs at Kommos indicates that these could have been deposited by either storm or tsunami waves, whereas at Lakki it is probably more likely that a tsunami resulted in the emplacement of the observed blocks but a storm cannot be ruled out. The most compelling site for having been the result of tsunami deposition is those boulders seen at Diplomo Petris. The large size, geomorphic characteristics and orientation are all strongly indicative of tsunami transport, most likely by the 365 CE tsunami. Radiocarbon dating from Lakki is also consistent with the 365 CE tsunami. Although, fine-grained deposits have been identified for this event (i.e., Scheffers & Scheffers, 2007), these are the first coarse-grained material identified on Crete resulting from this large event. Given that large magnitude earthquakes and tsunamis are infrequent in the Mediterranean basin these observations provide important data to inform and test models of tsunami occurrence and risk in this populous region.

Acknowledgements

This project was supported by a fieldwork grant from the Geological Society of London. Thanks to the Institute of Oceanography and Y. Antoniou, Hellenic Centre for Marine Research for providing the wave data from the POSEIDON Operational Oceanography System (http://www.poseidon.hcmr.gr). The Landsat data was obtained through the Global Land Cover Facility, University of Maryland (http://glcf.umd.edu/). We also thank the Ellie Scourse and two anonymous reviewers for useful comments that have improved the manuscript.

Appendix A. Boulder transport equations

For all equations the variables are as follows:

H is the wave height at breaking point, H_s denotes storm waves and H_t denotes tsunami waves,

ρ_s = density of the boulder (Table 1),

ρ_w = density of water (1.02 g/cm^3),

a = A-axis of the boulder,

b = B-axis of the boulder,

c = C-axis of the boulder,

C_D = coefficient of drag (1.2) (*cf.*, Benner *et al*., 2010),

C_L = coefficient of lift (0.178) (*cf.*, Noormets *et al*., 2011),

C_m = coefficient of mass (2),

μ = coefficient of friction (0.65)

ü = instantaneous flow acceleration (1 m/s^2),

u = velocity of a wave (m/s)

g = acceleration due to gravity (9.81 m/s^2).

Θ = Angle of beach

Nandasena *et al*. (2011)

Submerged boulder – Sliding

$$u^2 \geq \frac{2(\rho_s / \rho_w - 1)gc(\mu \cos\theta + \sin\theta)}{C_d(c/b) + \mu_s C_l}$$

Submerged boulder – Rolling

$$u^2 \geq \frac{2(\rho_s / \rho_w - 1)gc(\cos\theta + (c/b)\sin\theta)}{C_d(c^2/b^2) + C_l}$$

Subaerial Boulder

$$u^2 \geq \frac{2\left(\rho_b/\rho_w - 1\right)g\left(bc^2 \sin\theta + b^2 c \cos\theta\right) - 2C_m\left(bc^2\right)\dot{u}}{C_d c^2 + C_l b^2}.$$

Joint-bounded Boulder

$$u^2 \geq \frac{2(\rho_s / \rho_w - 1)gc(\cos\theta + \mu_s \sin\theta)}{C_l}$$

Benner *et al*. (2010)

Submerged boulder

$$Ht \geq \frac{0.5bc[b(p_s - p_w)/p_w - (p_s C_m \ddot{u}c)/(p_w g)]}{C_D c^2 + C_L b^2}$$

$$Hs \geq \frac{2bc[b(p_s - p_w)/p_w - (p_s C_m \ddot{u}c)/(p_w g)]}{C_D c^2 + C_L b^2}$$

Pignatelli *et al*. (2009)

Joint-bounded boulders

$$Ht \geq \frac{0.25c[(p_s - p_w)/p_w]}{C_L}$$

$$Hs \geq \frac{2c[(p_s - p_w)/p_w]}{C_L}$$

Barbano *et al*. (2010)

Submerged boulder

$$Ht \geq \frac{[((p_s - p_w)/p_w)b^2 c\ ]}{2(C_D c^2 + C_L b^2)}$$

$$Hs \geq \frac{[((p_s - p_w)/p_w)b^2 c\ ]}{0.5(C_D c^2 + C_L b^2)}$$

Subaerial Boulder

$$Ht \geq \frac{[0.5(p_s - p_w/p_w)b^2 c\, g - C_m\, bc^2 \ddot{u}]}{g(C_D c^2 + C_L b^2)}$$

$$Hs \geq \frac{[2(p_s - p_w/p_w)b^2 c\, g - 4C_m\, bc^2 \ddot{u}]}{g(C_D c^2 + C_L b^2)}$$

Joint-bounded Boulder

$$Ht \geq \frac{0.5c[(p_s - p_w)/p_w]}{C_L}$$

$$Hs \geq \frac{2c[(p_s - p_w)/p_w]}{C_L}$$

References

Ambraseys N, & Synolakis C. 2010. Tsunami catalogs for the Eastern Mediterranean, revisited. Journal of Earthquake Engineering, 14, 309–330.

Bahlburg, H. & Spiske, M., 2012. Sedimentology of tsunami inflow and backflow deposits: key differences revealed in a modern example. Sedimentology 59 (3), 1063-1086

Barbano, M.S., Pirrotta, C., & Gerardi, F., 2010. Large boulders along the south-eastern Ionian coast of Sicily: storm or tsunami deposits? Marine Geology, 275, 140-154.

Benner, R., Browne, T., Brückner, H., Kelletat, D., & Scheffers, A., 2010. Boulder transport by waves: progress in physical modelling. Zeitschrift für Geomorphologie, Supplementary Issues, 54(3), 127-146.

Blair, T.C., & McPherson, J.G., 1999. Grain-size and textural classification of coarse sedimentary particles. Journal of Sedimentary Research, 69, 6-19.

Bruins, H.J., MacGillivray, J.A., Synolakis, C.E., Benjamini, C., Keller, J., Kisch, H.J., Klügel, A., & van der Plicht, J., 2008. Geoarchaeological tsunami deposits at Palaikastro (Crete) and the Late Minoan IA eruption of Santorini. Journal of Archaeological Science, 35, 191-212.

Bryant, E.A. & Nott, J., 2001. Geological indicators of large tsunami in Australia. Natural Hazards. 24, 231-249.

Butler, A., Heffernan, J.E., Tawn, J.A., Flather, R.A. & Horsburgh, K.J., 2007. Extreme value analysis of decadal variations in storm surge elevations. Journal of Marine Systems, 67, 189-200.

Cavaleri, L., & Sclavo, M., 2006. The calibration of wind and wave model data in the Mediterranean Sea. Coastal Engineering, 53(7), 613-627.

Coles, S., 2001. An introduction to Statistical Modelling of Extreme Values. Springer. London, U.K. pp 208

Dally, W.R., 2005. Surf zone processes. In: Schwartz, M.L. (ed.): Encyclopedia of Coastal Science: 929-935. Dordrecht.

Dawson A.G., 1994. Geomorphological effects of tsunami run-up and backwash. Geomorphology, 10, 83–94.

Dawson, A.G. & Shi S., 2000. Tsunami deposits. Pure and Applied Geophysics, 157, 875–897

Deutsches Hydrographisches Institut (DHI), 1971. Mittelmeer-Handbuch. 4. Teil: Griechenland und Kreta. 5. Auflage

Dominey-Howes, D. T. M., 1998. Assessment of tsunami magnitude and implications for urban hazard planning in Greece. Disaster Prevention and Management: An International Journal, 7(3), 176-182.

Dominey-Howes, D., 2004. A re-analysis of the Late Bronze Age eruption and tsunami of Santorini, Greece, and the implications for the volcano-tsunami hazard. Journal of Volcanism and Geothermal Research, 130 (1-2), 107-132.

Dominey-Howes, D. T. M., Papadopoulos, G. A., & Dawson, A. G., 2000. Geological and historical investigation of the 1650 Mt. Columbo (Thera Island) eruption and tsunami, Aegean Sea, Greece. Natural Hazards, 21(1), 83-96.

Engel, M. & May, S. M., 2012. Bonaire's boulder fields revisited: evidence for Holocene tsunami impact on the Leeward Antilles. Quaternary Science Reviews 54, 126-141.

England, P., Howell, A., Jackson, J. & Synolakis, C., 2015. Palaeotsunamis and tsunami hazards in the Eastern Mediterranean. Philosophical Transactions of the Royal Society A 373: 20140374.

Etienne, S. & Paris, R., 2010. Boulder accumulations related to storms on the Reykjanes Peninsula, Iceland. Geomorphology, 114, 55-70.

Etienne, S., Buckley, M., Paris, R., Nandasena, A.K., Clark, K., Strotz, L., Chague-Goff, C., Goff, J. & Richmond, B., 2011. The use of boulders for characterising past tsunamis: Lessons from the 2004 Indian Ocean and 2009 South Pacific tsunamis. Earth Science Reviews, 107, 76-90.

EurOtop, 2007. Wave overtopping of sea defences and related structures: Assessment Manual. Die Küste, 73, 178 pp.

Ganas, A. & Parsons, T., 2009. Three-dimensional model of Hellenic Arc deformation and origin of the Cretan uplift. Journal of Geophysical. Research-Solid Earth, 114, B06404.

Gilleland, E., & Katz, R. W., 2006. Analyzing seasonal to interannual extreme weather and climate variability with the extremes toolkit (extRemes), 18th Conference on Climate Variability and Change, 86th American Meteorological Society (AMS) Annual Meeting, 29 January - 2 February, 2006, Atlanta, Georgia. pp 2.15.

Goff, J.R., Dudley, W.C., de Maintenon, M.J., Cain, C. & Coney, J.P., 2006. The largest local tsunami in 20th century Hawaii. Marine Geology, 226, 65-79.

Goto, K., Chavanich, S. A., Imamura, F., Kunthasap, P., Matsui, T., Minoura, K., Sugawara, D., & Yanagisawa, H., 2007. Distribution, origin and transport process of boulders deposited by the 2004 Indian Ocean tsunami at Pakarang Cape, Thailand. Sedimentary Geology, 202(4), 821-837.

Goto, K., Shinozaki, T., Minoura, K., Okada, K., Sugawara, D. & Imamura, F., 2010. Distribution of boulders at Miyara Bay of Ishigaki Island, Japan: A flow characteristic indicator of tsunami and storm waves. Island Arc, 19, 412-426.

Goto, K.,Sugawara, D., Ikema, S. & Miyagi, T., 2012. Sedimentary processes associated with sand and boulder deposits formed by the 2011 Tohoku-oki tsunami at Sabusawa Island, Japan. Sedimentary Geology, 282, 1-13.

Guidoboni, E. & Comastri, A., 1997: The large earthquake of 8 August 1303 in Crete: seismic scenario and tsunami in the Mediterranean area. Journal of Seismology 1, 55-72.

Guidoboni, E., Comastri, A., & Traina, G., 1994. Catalogue of Ancient Earthquakes in the Mediterranean Area up to the 10th Century (Vol. 1). SGA.

Hoffman, G., Reicherter, K., Wiatr, T., Grützner, C. & Rausch, T., 2013. Block and boulder accumulations along the coastline between Fins and Sur (Sultanate of Oman): tsunamigenic remains? Natural Hazards, 65, 851-873.

Hoffmeister, D., Tilly, N., Curdt, C., Aasen, H., Ntageretzis, K., Hadler, H., Willerhäuser, T., Vött, A., & Bareth, G., 2012. Terrestrial laser scanning for coastal geomorphologic research in Western Greece. International Archives of the Photogrammetry, Remote Sensing and Spatial Information Sciences, 39(B5), 511-516.

Imamura, F., Goto, K. & Ohkubo, S., 2008. A numerical model for the transport of a boulder by tsunami. J. Geophys. Res. 113, C01008. doi:10.1029/2007JC004170.

Kelletat, D. & Schellmann, G., 2002. Tsunamis on Cyprus – field evidences and ^{14}C dating results. Zeitschrift fur Geomorpholgie, NF 46, 19-34.

Kelletat, D., Scheffers, A. & Scheffers, S., 2004. Holocene tsunami deposits on the Bahaman Islands of Long Island and Eleuthera. Zeitschrift fur Geomorpholgie, 48, 519-540.

Kennedy, D.M., Tannock, K.L., Crozier, M.J. & Rieser, U., 2007. Boulders of MIS 5 age deposited by a tsunami on the coast of Otago, New Zealand. Sedimentary Geology, 200, 222-231.

Kortekaas, S., & Dawson, A. G., 2007. Distinguishing tsunami and storm deposits: an example from Martinhal, SW Portugal. Sedimentary Geology, 200(3), 208-221.

Lau, A. A., Terry, J. P., Switzer, A. D., & Pile, J., 2015. Advantages of beachrock slabs for interpreting high-energy wave transport: Evidence from Ludao Island in south-eastern Taiwan. Geomorphology, 228, 263-274.

Mastronuzzi, G., & Sansò, P., 2004. Large boulder accumulations by extreme waves along the Adriatic coast of southern Apulia (Italy). Quaternary International, 120(1), 173-184.

May, S.M., Vött, A., Bruckner, H. & Smedile, A., 2012. The Gyra washover fan in the Lefkada Lagoon, NW Greece – possible evidence of the 365AD Crete earthquake and tsunami. Earth, Planets and Space, 64, 859 – 874.

May, S. M., Engel, M., Brill, D., Cuadra, C., Lagmay, A. M. F., Santiago, J., Suarez, J. K., Reyes, M., Brückner, H., 2015. Block and boulder transport in Eastern Samar (Philippines) during Supertyphoon Haiyan. Earth Surface Dynamics Discussions 3, 739-771.

Maouche, S., Morhange, C. & Meghraoui, M., 2009. Large boulder accumulation on the Algerian coast evidence tsunami events in the western Mediterranean. Marine Geology., 262, 96-104.

Morton, R. A., Gelfenbaum, G. & Jaffe, B. E., 2007. Physical criteria for distinguishing sandy tsunami and storm deposits using modern examples. Sedimentary Geology, 200(3), 184-207.

Morton, R. A., Richmond, B. M., Jaffe, B. E. & Gelfenbaum, G., 2008. Coarse-clast ridge complexes of the Caribbean: a preliminary basis for distinguishing tsunami and storm-wave origins. Journal of Sedimentary Research, 78(9), 624-637.

Mottershead, D., Bray, M., Soar, P., & Farres, P. J., 2014. Extreme wave events in the central Mediterranean: Geomorphic evidence of tsunami on the Maltese Islands. Zeitschrift für Geomorphologie, 58(3), 385-411.

Mottershead, D. N., Bray, M. J., Soar, P. J., & Farres, P. J., 2015. Characterisation of erosional features associated with tsunami terrains on rocky coasts of the Maltese islands. Earth Surface Processes and Landforms, 40 , 2093-2111.

Nandasena, N. A. K., Paris, R. & Tanaka, N., 2011. Reassessment of hydrodynamic equations: Minimum flow velocity to initiate boulder transport by high energy events (storms, tsunamis). Marine Geology 281, 70-84.

Nandasena, N. A. K., Tanaka, N., Sasaki, Y., & Osada, M., 2013. Boulder transport by the 2011 Great East Japan tsunami: Comprehensive field observations and whither model predictions? Marine Geology, 346, 292-309.

NASA Landsat Program, 2003, Landsat ETM+ scene p182r036_7dt20000630_z34, SLC-Off, USGS, 10/26/2003.

National Geophysical Data Center / World Data Service (NGDC/WDS): Global Historical Tsunami Database. National Geophysical Data Center, NOAA. doi:10.7289/V5PN93H7 [accessed on: 23/02/2015]

Nocquet J-M., 2012. Present-day kinematics of the Mediterranean: a comprehensive overview of GPS results. Tectonophysics 579, 220–242.

Noormets, R., Crook, K.A.W. & Felton, E.A., 2004. Sedimentology of rocky shorelines: 3. Hydrodynamics of megaclast emplacement and transport on a shore platform, Oahu, Hawaii. Sedimentary Geology. 172, 41-65.

Nott, J., 1997. Extremely high-energy wave deposits inside the Great Barrier Reef, Australia: determining the cause – tsunami or tropical cyclone. Marine Geology 141, 193-207.

Nott, J., 2003a. Tsunami or Storm Waves? – Determining the origin of spectacular field of wave emplaced boulders using numerical storm surge and wave models and hydrodynamic transport equations. Journal of Coastal Research, 19, 348-356.

Nott, J., 2003b. Waves, coastal boulder deposits and the importance of the pre-transport setting. Earth and Planetary Science Letters, 210, 269-276.

Oak, H.L., 1984. The boulder beach, a fundamentally distinct sedimentary assemblage (New South Wales, Australia). Annals of the Association of American Geographers, 74, 71-82.

Papadimitriou E.E. & Karakostas V.G., 2008. Rupture model of the great AD 365 Crete earthquake in the southwestern part of the Hellenic Arc. Acta Geophysica, 56, 293–312.

Paris, R., Wassmer, P., Sartohadi, J., Lavigne, F., Barthomeuf, B., Desgages, E., Grancher, D., Baumert, P., Vautier, F., Brunstein, D. & Gomez, C., 2009. Tsunamis as geomorphic crises: lessons from the December 26, 2004 tsunami in Lhok Nga, West Banda Aceh (Sumatra, Indonesia). Geomorphology, 104, 59-72.

Paris, R., Fournier, J., Poizot, E., Etienne, S., Morin, J., Lavigne, F. & Wassmer, P., 2010. Boulder and fine sediment transport and deposition by the 2004 tsunami in Lhok Nga (western Banda Aceh, Sumatra, Indonesia): A coupled offshore–onshore model. Marine Geology, 268, 43-54.

Paris, R., Naylor, L.A. & Stephenson, W.J., 2011. Boulders as a signature of storms on rock coasts. Marine Geology, 283, 1-11.

Phuwieng, P., Imamura, F., & Koshimura, S., 2008. The correlation between tsunami run-up height and coastal characteristics index of Phang Nga and Phukey Provinces, Thailand. Bulletin of the International Institute of Seismology and Earthquake Engineering, 42, 145-150.

Pignatelli, C., Sansò, P., & Mastronuzzi, G., 2009. Evaluation of tsunami flooding using geomorphologic evidence. Marine Geology, 260(1), 6-18.

Pirazzoli, P.A., 1986. The Early Byzantine tectonic paroxysm. Zeitschrift für Geomorphologie, NF Suppliment. 62, 31-49.

Pirazzoli, P. A., Ausseil‐Badie, J., Giresse, P., Hadjidaki, E., & Arnold, M., 1992. Historical environmental changes at Phalasarna harbor, West Crete. Geoarchaeology, 7(4), 371-392.

Pirazzoli, P. A., Laborel, J., & Stiros, S. C., 1996. Earthquake clustering in the Eastern Mediterranean during historical times. Journal of Geophysical Research: Solid Earth (1978–2012), 101(B3), 6083-6097.

Pope, R., Wilkinson, K., Skourtsos, E., Triantaphyllou, M. & Ferrier, M., 2008. Clarifying stages of alluvial fan evolution along the Sfakian piedmont, southern Crete: New evidence from analysis of post-incisive soils and OSL dating. Geomorphology 94 (1-2), 206-225.

Ramalho, R. S., Winckler, G., Madeira, J., Helffrich, G. R., Hipólito, A., Quartau, R., Adena, K., & Schaefer, J. M., 2015. Hazard potential of volcanic flank collapses raised by new megatsunami evidence. Science Advances, 1(9), e1500456.

Reilinger, R., McClusky, S., Vernant, P., Lawrence, S., Ergintav, S., Cakmak, R., Ozener, H., Kadirov, F., Guliev, I., Stepanyan, R., Nadaria, M., Hahubia, G., Mahmoud, S., Sakr, K., ArRajehi, A., Paradissis, D., Al-Aydrus, A., Prilepin, M., Guseva, T., Evren, E., Dmitrotsa, A., Filikov, S.V., Gomez, F., Al-Ghazzi, R., & Karam, G., 2006. GPS constraints on continental deformation in the Africa‐Arabia‐Eurasia continental collision zone and implications for the dynamics of plate interactions. Journal of Geophysical Research: Solid Earth (1978–2012), 111(B5).

Reilinger, R., McClusky, S., Paradissis, D., Ergintav, S., & Vernant, P. (2010). Geodetic constraints on the tectonic evolution of the Aegean region and strain accumulation along the Hellenic subduction zone. Tectonophysics, 488(1), 22-30.

Reimer, P. J., Bard, E., Bayliss, A., Beck, J. W., Blackwell, P. G., Bronk Ramsey, C., & van der Plicht, J., 2013. IntCal13 and Marine13 radiocarbon age calibration curves 0-50,000 years cal BP. University of Arizona.

Richmond, B. M., Buckley, M., Etienne, S., Chagué-Goff, C., Clark, K., Goff, J., Dominey-Howes, D. & Strotz, S., 2011a. Deposits, flow characteristics, and landscape change resulting from the September 2009 South Pacific tsunami in the Samoan islands, Earth-Science Reviews, 107, 38-51.

Richmond, B.M., Watt, S., Buckley, M.L, Jaffe, B.E., Gelfenbaum, G., & Morton, 2011b, Recent storm and tsunami coarse-clast deposit characteristics, Southeast Hawaii, Marine Geology, 283, 79-89

Scheffers, A., 2008. Tsuanmi boulder deposits. In: Shiki, T., Tsuji, Yamazaki, T., Minoura, K (eds), Tsunamiites: Features and Implications. Elsevier B.V., pp. 299-317.

Scheffers, A. & Scheffers, S., 2007. Tsunami deposits on the coastline of west Crete (Greece). Earth and Planetary Science Letters, 259, 613-624.

Scheffers, A., Kelletat, D., Vött, A., May, S.M., & Scheffers, S., 2008. Late Holocene tsunami traces on the western and southern coastlines of the Peloponnesus (Greece). Earth and Planetary ScienceLetters, 269, 271-279.

Scicchitano, G., Monaco, C. & Tortorici, L., 2007. Large boulder deposits by tsunami waves along the Ionian coast of south-eastern Sicily (Italy). Marine Geology 238: 75–91.

Shah-hosseini, M., Morhange, C., Beni, A., N., Marriner, N., Lahijani, H., Hamzeh, M., & Sabatier, F., 2011. Coastal boulders as evidence for high-energy waves of the Iranian coast of Makran. Marine Geology, 17-28.

Shaw, B., Ambraseys, N.N., England, P.C., Floyd, M.A., Gorman, G.J., Higman, T.F.G., Jackson, J.A., Nocquet, J,-M., Pain, C.C., & Piggott, M.D., 2008. Eastern Mediterranean tectonics and tsunami hazard inferred from the AD 365 earthquake. Nature Geoscience, 1, 268-276.

Smedile, A., De Martini, P. M., Pantosti, D., Bellucci, L., Del Carlo, P., Gasperini, L., Pirrotta, C., Polonia, A., & Boschi, E., 2011. Possible tsunami signatures from an integrated study in the Augusta Bay offshore (Eastern Sicily—Italy). Marine Geology, 281(1), 1-13.

Smedile, A., De Martini, P. M., & Pantosti, D., 2012. Combining inland and offshore paleotsunamis evidence: the Augusta Bay (eastern Sicily, Italy) case study. Natural Hazards and Earth System Science. 12, 2557-2567.

Smith, R. L., 1986. Extreme value theory based on the r largest annual events. Journal of Hydrology, 86, 27 – 43.

Spiske, M., Böröcz, Z. & Bahlburg, H., 2008. The role of porosity in discriminating between tsunami and hurricane emplacement of boulders - a case study from the Lesser Antilles, southern Caribbean. Earth and Planetary Science Letters 3-4, 384-396.

Stiros, S. C., & Papageorgiou, S., 2001. Seismicity of western Crete and the destruction of the town of Kisamos at AD 365: archaeological evidence. Journal of Seismology, 5(3), 381-397.

Stiros, S. C., 2010. The 8.5+ magnitude, AD365 earthquake in Crete: Coastal uplift, topography changes, archaeological and historical signature. Quaternary International, 216(1), 54-63.

Stuiver, M., & Reimer, J., 1993. Extended 14C data base and revised CALIB 3.014 C age calibration program. Radiocarbon, 35, 215-230.

Tawn, J.A. & Vassie, J. M., 1990. Spatial transfer of extreme sea-level data for use in revised joint probability method. Proceedings of the Institute of Civil Engineering, Part 2, 89, 433 – 438.

ten Veen, J.H., & Kleinspehn, K.L., 2003. Incipient continental collision and plate-boundary curvature; late Pliocene-Holocene transtensional Hellenic forearc, Crete, Greece. Journal of the Geological Society of London, 160(2):161-181

Titov, V.V., & Synolakis, C.E., 1997. Extreme inundation flows during the Hokkaido-Nansei-Oki Tsunami. Geophysical Research Letters, 24, 1315–1318.

Tortorici, L., Catalano, S., Cirrincione, R. & Tortorici, G., 2012. The Cretan ophiolite-bearing mélange (Greece): A remnant of Alpine accretionary wedge. Tectonophysics, 568, 320-334.

Vacchi, M. Rovere, A., Zouros, N. & Firpo M., 2012. Assessing enigmatic boulder deposits in NE Aegean Sea: importance of historical sources as tool to support hydrodynamic equations. Natural Hazards and Earth Systems Science, 12, 1109 – 1118.

Vella, C. Demory, F. Canut, V. Dussouillez, P. & Fleury T. J., 2011. First evidence of accumulation of mega boulders on the Mediterranean rocky coast of Provence (southern France). Natural Hazards and Earth Systems Science, 11, 905–914.

Vernant, P., Reilinger, R., & McClusky, S. 2014 Geodetic evidence for low coupling on the Hellenic subduction plate interface. Earth & Planetary Science Letters 385, 122–129.

Vött, A., Bareth, G., Brückner, H., Curdt, C., Fountoulis, I., Grapmayer, R., Hadler, H., Hoffmeister, D., Klasen, N., Lang, F., Masberg, P., May, S. M., Ntageretzis, K., Sakellariou, D., &

Willershaüer, T., 2007. Beachrock-type calcarenitic tsunamites along the shores of the eastern Ionian Islands and the western Peloponnese. Zeitschrift für Geomorphologie, 54, Suppl. 3. 1-50.

Vött, A. Brückner, H. May, M. Lang, F. Herd, R &. Brockmüller, S. 2008. Strong tsunami impact on the Bay of Aghios Nikolaos and its environs (NW Greece) during Classical–Hellenistic times, Quaternary International, 181 (1), 105-122

Vött, A., Brückner, H., Brockmüller, S., Handl, M., May, S.M., Gaki-Papanastassiou, K., Herd, R., Lang, F., Maroukian, H., Nelle, O., & Papanastassiou, D., 2009. Traces of Holocene tsunamis across the Sound of Lefkada, NW Greece, Global and Planetary Change, 66 (1–2), 112-128.

Vött, A., Lang, F., Brückner, H., Gaki-Papanastassiou, K., Maroukian, H., Papanastassiou, D., Giannikos, A., Hadler, H., Handl, M., Ntageretzis, K., Willershäuser, T., & Zander, A., 2011. Sedimentological and geoarchaeological evidence of multiple tsunamigenic imprint on the Bay of Palairos-Pogonia (Akarnania, NW Greece), Quaternary International, 242, 213-239.

Whitworth, M.R.Z., 2015. Utilising probabilistic techniques in the assessment of extreme coastal flooding frequency-magnitude relationships using a case study from south-west England. PhD Thesis, University of Plymouth.